

1 Identifying the components of the solid–electrolyte interphase in Li-ion Batteries

2

3 Luning Wang¹, Anjali Menakath², Fudong Han³, Yi Wang¹, Peter Y. Zavalij¹, Karen Gaskell¹, Oleg Borodin⁴, Dinu Iuga², Steven P.
4 Brown², Chunsheng Wang^{1,3*}, Kang Xu^{4*} and Bryan W. Eichhorn^{1*}

5

6 ¹*Department of Chemistry and Biochemistry, University of Maryland, College Park, MD 20742, USA*

7 ²*Department of Physics, University of Warwick, Coventry, CV4 7AL, United Kingdom*

8 ³*Department of Chemical and Biomolecular Engineering, University of Maryland, College Park, MD 20742, USA*

9 ⁴*Electrochemistry Branch, Power and Energy Division Sensor and Electron Devices Directorate, U.S. Army Research Laboratory,*
10 *Adelphi, MD 20783, USA*

11

12 **Abstract**

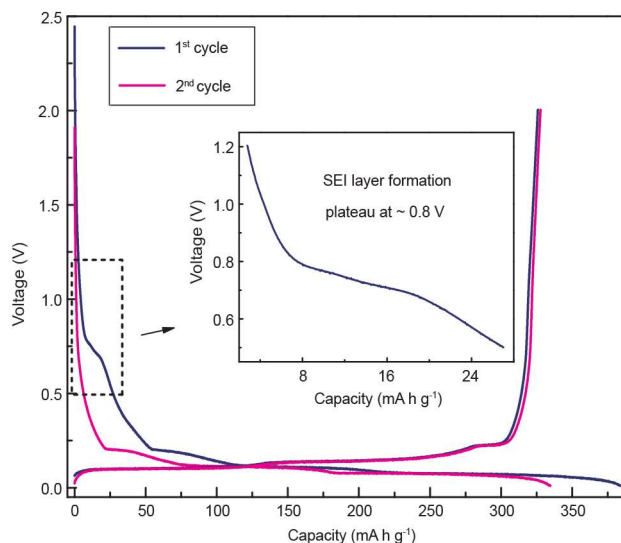
13 The importance of the solid–electrolyte interphase (SEI) for reversible operation of Li-ion batteries (LIBs) has been well-
14 established, but understanding of its chemistry remains incomplete. The current consensus on the identity of the major organic
15 SEI component is that it consists of lithium ethylene di-carbonate (LEDC), which is thought to have a high Li-ion conductivity but
16 a low electronic conductivity to protect the Li/C electrode. We report here on the synthesis, structural and spectroscopic
17 characterizations of authentic LEDC and lithium ethylene mono-carbonate (LEMC). Direct comparisons of SEI grown on graphite
18 anodes suggest that LEMC, instead of LEDC, is likely the major SEI component. Single crystalline X-ray diffraction (XRD) studies on
19 LEMC and lithium methyl carbonate (LMC) reveal unusual layered structures and Li⁺ coordination environments. LEMC has Li⁺
20 conductivities of above 10⁻⁶ S/cm, while LEDC is almost an ionic insulator. The complex interconversions and equilibria of LMC,
21 LEMC and LEDC in dimethyl sulfoxide (DMSO) solutions are also investigated.

22

1 Introduction

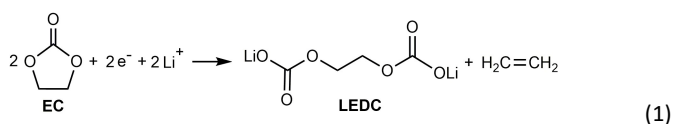
2 Li-ion batteries (LIBs) are ubiquitous in 21st century life and have an estimated 2018 global market of US\$ 25 billion.
3 Despite their technological importance and mass production, a molecular level understanding of ion transport mechanisms and
4 the interfacial chemistry in these devices remain elusive. As evidenced by the history of LIBs,¹ misconceptions in fundamental
5 chemistries often delay breakthroughs in new materials, for which interphases on graphite anodes are a conspicuous example.
6 Graphitic materials serve as the standard anodes in the current LIBs. In the charge and discharge processes of a LIB, Li⁺ intercalates
7 into and de-intercalates from the graphene layers.²⁻⁷ Due to the extremely low potentials where such intercalation/de-
8 intercalation processes occur (~ 0.2 V vs. Li⁺/Li),^{4,8,9} commonly used carbonate-based electrolytes (*e.g.* 1 M LiPF₆ in ethylene
9 carbonate (EC)/dimethyl carbonate (DMC)) are electrochemically reduced at the anode surface in the first few charge/discharge
10 cycles.⁹⁻¹¹ This electrochemical reduction generates an insoluble passivating film on the anode surface known as the solid-
11 electrolyte interphase (SEI),¹²⁻¹⁶ which constitutes a critical component of LIBs in that it prevents further parasitic electrolyte
12 decomposition and stabilizes battery operation and capacity.^{7,12,13} The SEI is still regarded as one of the most important but the
13 least understood component in rechargeable LIBs although extensive efforts have been devoted to elucidating its composition
14 and function.¹⁷ While it is well accepted that the SEI is approximately 10 - 50 nm thick,^{7,14,18-23} contains inorganic salts (*e.g.* Li₂CO₃
15 and LiF),^{14,18,20,24,25} degraded carbonate molecules (semi-carbonates and polymers),^{10,15,24,26-32} and prevents further solvent
16 degradation as an electronic insulator while facilitating Li⁺ transport as an electrolyte,^{7,12,13} the precise structure, composition
17 and the functional mechanism(s) of the SEI remain under debate.

18 It is well accepted that the organic SEI component primarily comes from electrochemical reduction of EC, as is often
19 evidenced by a narrow shoulder in the discharge curve at *ca.* 0.8 V during the first discharge cycle (Fig. 1).^{13,33,34} The importance
20 of EC-originated products in the SEI is evidenced by the necessity of employing EC in essentially all commercial electrolytes, where
21 preferential solvation of Li⁺ by EC dictates SEI formation.^{35,36} EC reduction is commonly believed to react via a “single-electron
22 pathway” that generates lithium ethylene di-carbonate (LEDC) according to equation (1).^{10,15,26,28,37} Identification of LEDC in
23 authentic nanoscopic SEI films has been accomplished through multiple spectroscopic techniques including X-ray photoelectron
24 spectroscopy (XPS),^{10,14,33} Fourier-transform infrared spectroscopy (FTIR),^{10,15,26,28,31,33,38} solid-state and solution phase nuclear
25 magnetic resonance (NMR) spectroscopy,^{14,32,39,40} to name a few. The SEI spectroscopic signatures were compared to those of
26 synthetic LEDC standards, which have been independently reported by four separate laboratories, including one of us.^{37,39,41,42}
27 Unfortunately, these synthetic procedures for LEDC synthesis suffer from insolubility problems that lead to kinetic limitations in
28 the carbonate formation process. Herein we report that these reported synthetic standards are not LEDC but are actually lithium
29 ethylene mono-carbonate (LEMC) and, to our knowledge, LEDC has not been prepared prior to our work.



1
2 Figure 1. Electrochemical behavior of a graphite electrode. The dark blue and red curves show the 1st and 2nd battery cycles,
3 respectively, with 1M LiPF₆ in EC/DMC (v: v = 1: 1) as electrolyte solution and Li foil as the counter electrode. The inset indicates
4 formation of SEI layers at a plateau of ~ 0.8 V in the 1st lithiation process of the graphite electrode.
5

6 We describe here high-yield synthetic routes to LEDC•2DMSO, LEMC and lithium methyl carbonate (LMC). These
7 compounds have been fully characterized using FTIR, 1D and 2D solution and solid-state NMR spectroscopy (¹H, ¹³C and ⁷Li), as
8 well as powder X-ray diffraction (XRD) for all compounds and single crystal X-ray studies for LEMC and LMC. In addition, we also
9 show that LEMC is a facile Li⁺ ion conductor whereas LEDC and LMC are not. Spectroscopic comparisons between authentic
10 EC/DMC derived SEI films and the synthetic model compounds suggest that the SEI likely contains an “LMC-capped LEMC organic
11 layer” and it is *unlikely* that LEDC is present in the SEI at all.



14 Results and discussion

15 **Synthesis and characterization.** LEMC was conveniently prepared in high yield as a white polycrystalline solid through the
16 lithiation/deprotonation of ethylene glycol (EG) with n-BuLi according to Fig. 2a. Single crystals of LEMC were obtained from EG
17 solutions layered with pyridine in *ca.* 10% yield. LMC was prepared in high yield in a similar manner, according to published
18 procedures (Fig. 2b).^{37,39,41} Single crystals of LMC were grown from a MeOH/Et₂O solution in *ca.* 30% yield. Synthetic details for
19 both compounds are given in the supplementary information along with full spectroscopic, analytical and structural data (FTIR,
20 solution and solid-state NMR, elemental analysis, powder and single crystal X-Ray diffraction, XPS, Supplementary Fig. 1 – 10 and
21 Supplementary Table 1 - 5). These white crystalline solids are soluble in rigorously dried DMSO but insoluble in ethereal and
22 hydrocarbon solvents. LEMC is also soluble in dry EG, moderately moisture sensitive and will slowly decompose in air. LMC is
23 soluble in MeOH and dimethylformamide, is air/moisture sensitive and also undergoes hydrolysis in solution.

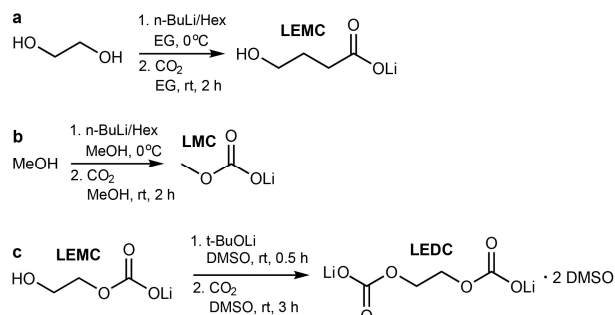


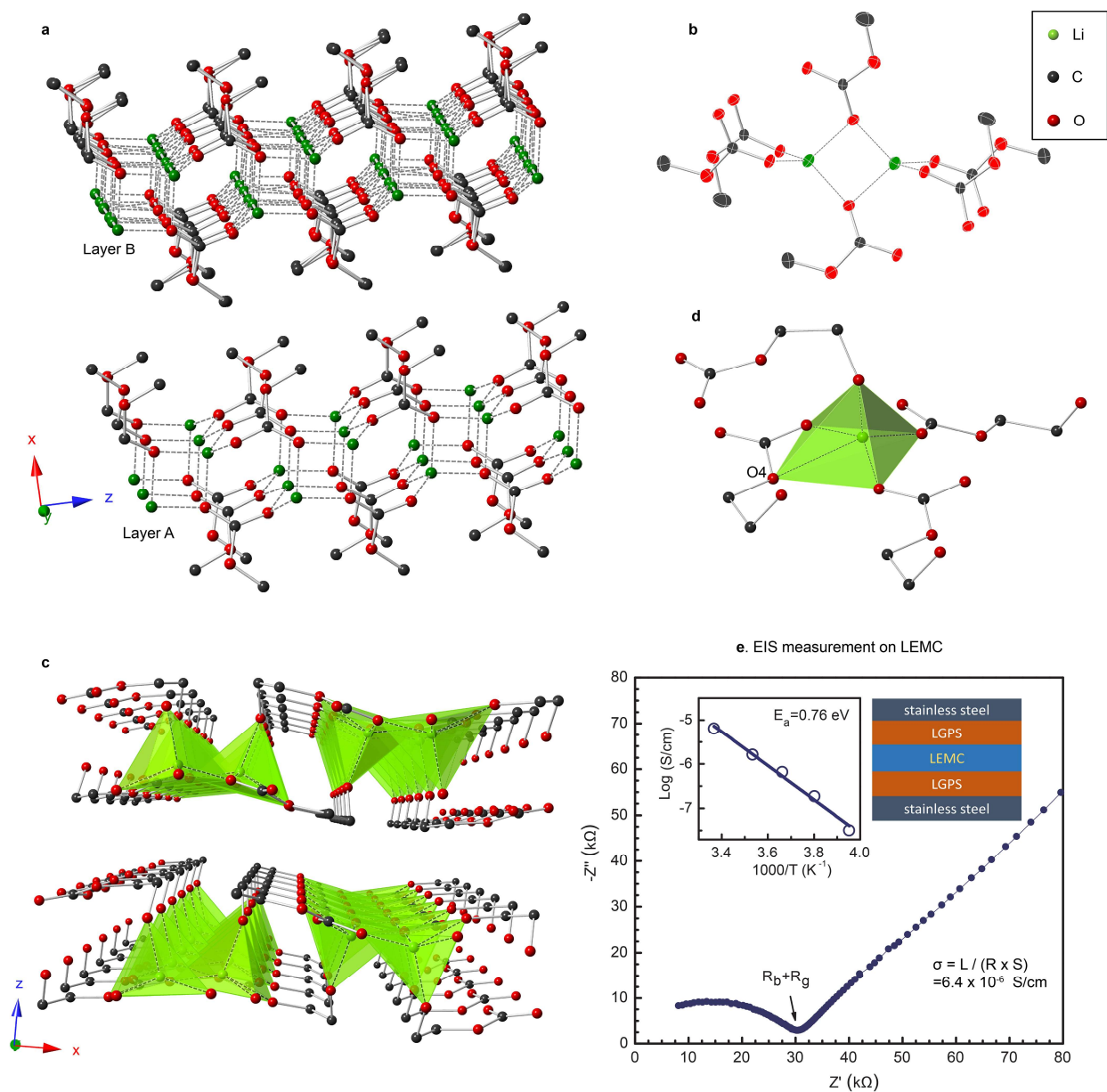
Figure 2. Chemical synthesis of (a) LEMC, (b) LMC and (c) LEDC·2DMSO.

Previous reports on the synthesis of "LEDC" involved nucleophilic addition of di-lithium ethylene glycolate (LiOCH₂CH₂OLi) to CO₂ in ethereal solvents.^{37,39,41} The reaction of EG with excess lithiation agents (n-BuLi or LiH) was expected to yield the di-lithium ethylene glycolate intermediate that subsequently reacts with CO₂ in ethereal solutions. However, it appears that the mono-lithiated intermediate, LiOCH₂CH₂OH (LiEG), is virtually insoluble in ethereal solvents and precipitates from solution before the second deprotonation can occur. We have found that addition of excess CO₂ (g) to the heterogeneous mixture results in an initial deactivation of the excess n-BuLi followed by a slower carbonate formation reaction with sparingly soluble LiOCH₂CH₂OH to give LEMC as the exclusive product. The experimental and calculated powder XRD and FTIR data for the analytically-pure LEMC single crystals from our studies are perfect matches to all previously reported data for "LEDC", indicating that these studies actually characterized LEMC (see Supplementary Fig. 11 - 12). With this knowledge, we employed the more convenient synthesis of LEMC involving direct deprotonation of EG with n-BuLi at 0°C, as described above in Fig. 2a.

Upon recognizing the solubility issues associated with the lithium glycolate intermediates, we devised an alternative synthesis of LEDC from LEMC in DMSO solutions. White polycrystalline LEDC·2DMSO was conveniently prepared through the deprotonation of LEMC by lithium tert-butoxide in DMSO, followed by reaction with excess CO₂ (Fig. 2c). The powder precipitates from solution in high yield and is slightly soluble in rigorously dry DMSO. The solid and its solutions are sensitive to moisture and other protic sources and are also air sensitive. Spectroscopic and analytical data (FTIR, solution and solid-state NMR, elemental analysis, see Supplementary Fig. 5 - 8) reveal a composition of LiOCO₂CH₂CH₂OCO₂Li·2(OSMe₂) or LEDC·2DMSO. To date, we have been unable to isolate single crystals of the compound and the precipitates give broad powder XRD profiles (Supplementary Fig. 1). Regardless, the analytical and spectroscopic data, specifically the NMR data (see below), unequivocally show that the compound is LEDC·2DMSO. Removal of DMSO solvates from the crystalline lattice of LEDC·2DMSO was accomplished by sonication in anhydrous THF at 50 °C, which generated amorphous LEDC as indicated by powder XRD and NMR studies (Supplementary Fig. 1 and 13).

Crystal structures of LEMC and LMC. The solid-state structures of LMC and LEMC were determined from single crystal X-ray studies of the respective crystals. Details of the refinements and crystallographic data are given in the supplementary information (crystallographic information file (CIF), Supplementary Table 2-3). LMC is monoclinic, space group *P*2₁/*c*, and contains two independent LMC molecules in the asymmetric unit that are partitioned into two different layers of the crystal lattice (see Fig. 3a and 3b). Layer A contains double sheets of LMC molecules with LiO₄ tetrahedra at the layer interior and the Me groups on the layer exterior. Each oxygen of the LiO₄ tetrahedra originates from a terminal carbonate oxygen of a different LMC molecule, two from each side of the layer, which links the structure into a two-dimensional network via edge-shared tetrahedra. While layer A is perfectly ordered, layer B has a 3:2 positional disorder in the y-z plane but is otherwise identical to A. The two layers alternately stack along the x-axis of the cell to give an unusual order - disorder - order layered structure of functionally identical

1



2

3 Figure 3. X-ray structures of LMC and LEMC, and EIS measurements on LEMC. Structures of LMC showing (a) the alternative
 4 packing of ordered Layer A and disordered Layer B and (b) the tetrahedral coordination of Li⁺ by O atoms. Structures of LEMC
 5 showing (c) the layers of LEMC double sheets and (d) the distorted pentagonal pyramidal 5-coordinate Li⁺ ion polyhedron. (e)
 6 shows the ionic conductivity of LEMC measured by EIS at 25 °C. The figure inset in (e) shows the linear fit used to calculate
 7 activation energy (E_a) for Li⁺ conductivity. The scheme shows the electrochemical cell used for the EIS measurements, where the
 8 LEMC layer was sandwiched between LGPS layers to block proton transfer. The ionic conductivity, σ, was calculated from the
 9 thickness of LEMC film, L, the resistance measured by EIS (R = R_b + R_g) and the area of LEMC in the cell, S.

10

11 subunits. The LiO₄ tetrahedra are somewhat distorted with Li-O bond distances that vary from 1.922 (6) - 2.011 (6) Å (ave. 1.960
 12 (2) Å) and O-Li-O angles that vary from 88.9 (3)° - 117.2 (3)°.

1 LEMC is orthorhombic, space group *Pbcn*, and contains a single unique molecule in the asymmetric unit. The structure
2 contains double sheets of LEMC molecules stacked along the z-axis of the orthorhombic cell (Fig. 3c and 3d), but the Li⁺ ions are
3 in distorted 5-coordinate pentagonal prismatic environments defined by three terminal carbonate oxygens, one alkyl carbonate
4 oxygen and an alcohol oxygen. Four of the Li-O bonds are typical (1.917 (8) - 2.027 (9) Å; ave. 1.996 (4) Å) with a longer 2.580 (9)
5 Å contact to the alkyl carbonate oxygen O4. The pentagonal prisms share corners to form double ribbons running in the y-
6 direction that are linked together in the x-direction by the spanning alcohol groups of the LEMC. Unlike the LMC structure, the
7 Li⁺ ions in LEMC reside in Li-O-Li-O lined crevices on the exterior of the layers. This unusual Li⁺ coordination geometry and its
8 position in the interlayer crevices of the layered lattice structure may play an important role in the Li⁺-ion conductivity described
9 below.

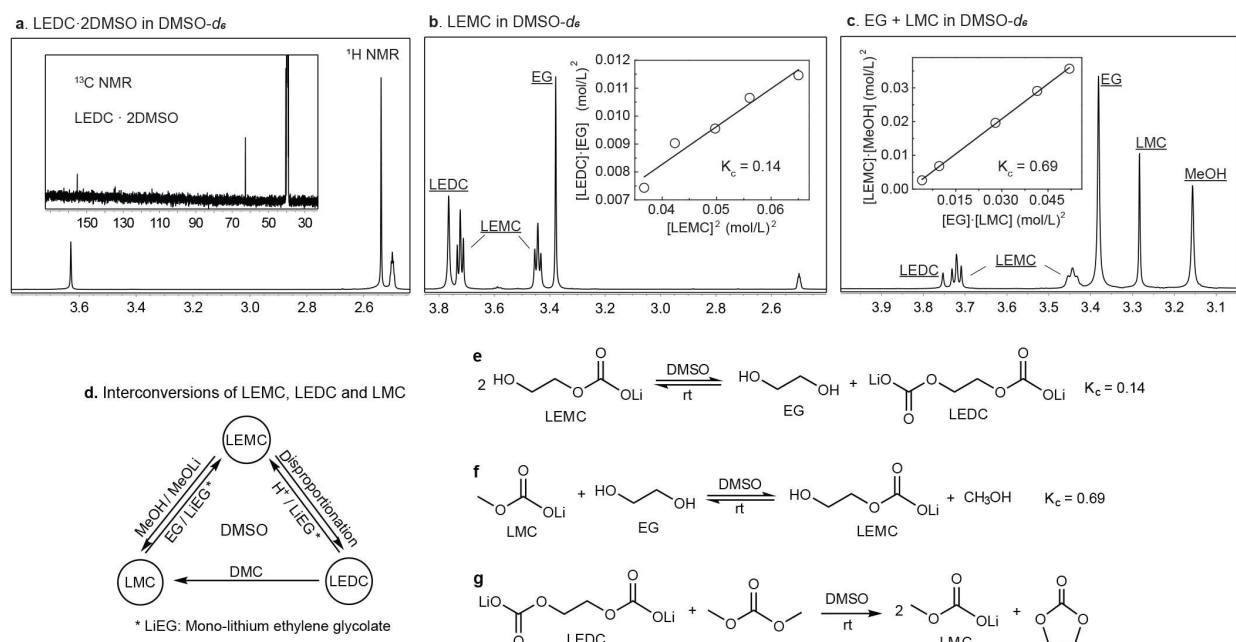
10 **Li-ion conductivities.** As both LMC and LEMC (reported as “LEDC” in prior publications) have been frequently reported as key
11 organic components of the SEI on graphite electrodes, information on their Li⁺ ion conductivities are thus of great importance
12 and are measured here by electrochemical impedance spectroscopy (EIS). Cold-pressed LEMC pellets are sandwiched between
13 two Li₁₀GeP₂S₁₂ (LGPS)^{43,44} rectifiers to block any proton conductivity during the measurements (See Methods for details). The EIS
14 data and the Arrhenius plot for Li⁺ conductivity of LEMC are shown in Fig. 3e. LEMC has reasonably high Li-ion conductivity of 6.4
15 x 10⁻⁶ S/cm at 25 °C, which is slightly better than single-domain LiPON films ($S \approx 3 \times 10^{-6}$ S/cm),⁴⁵ The activation energy (E_a) for
16 Li⁺ conductivity calculated from an Arrhenius analysis is 0.76 eV (Fig. 3e inset and Supplementary Fig. 14), which is higher than
17 common inorganic Li⁺ conductors but similar to organic-based Li⁺ ion conductors, such as LiClO₄/poly(ethylene oxide).^{43,45,46} The
18 influences of OH-rotation, Li⁺ interstitials, Li⁺ and H⁺ vacancies on the Li⁺ diffusion in LEMC were examined using Born
19 Oppenheimer molecular dynamics (BOMD) simulations of the superheated LEMC (Supplementary Figure 15-16). Addition of Li⁺
20 vacancy or Li⁺ substitution for H in the O-H groups results in the fastest Li⁺ diffusion, followed by Li⁺ interstitial diffusion occurring
21 via a “knock-off” mechanism²³ that is similar to Li₂CO₃, where the 5-fold Li-O coordination environment significantly decreases Li⁺
22 diffusion barriers.²³ Measurements on the amorphous LEDC and LMC (pressed pellets) give resistances outside the measurable
23 range, which we attribute to high resistivities (< 10⁻⁹ S/cm) of the two compounds. The high resistivity measured for LMC is
24 consistent with previous studies.⁴⁷

25 **Solution properties and NMR Studies.** In contrast to previous reports,^{41,48} our studies show that LEMC and LMC, as well as
26 LEDC·2DMSO, dissolve to give stable solutions in rigorously dry DMSO. However, all three compounds undergo aggregation in
27 the solution that leads to concentration-dependent chemical shifts in the ¹H, ¹³C and ⁷Li NMR spectra. Moreover, the compounds
28 are reactive towards water, residual solvent (MeOH, EG, EC or DMC) and are involved in complex equilibria and interconversions.
29 Details of the solution chemistry and the spectroscopic properties are given in Fig. 4, Supplementary Fig. 17 - 20, and will be
30 described in a subsequent publication. Only the pertinent properties are presented here.

31 Solution ¹H and ¹³C {¹H} NMR spectra for LEDC·2DMSO in DMSO-*d*₆ are given in Fig. 4a and Supplementary Fig. 5. Solid-
32 state 1D ¹H and ⁷Li magic-angle spinning (MAS) NMR spectra, along with 2D ¹H (SQ)-¹H (DQ) and ⁷Li-¹H MAS NMR spectra are
33 given in Supplementary Fig. 6 and 7. The 1D solid-state NMR spectra of LMC and LEMC simulated using the density-functional
34 theory (DFT) gauge-including projector-augmented wave (GIPAW) approach^{49,50} demonstrate high consistency with experimental
35 data (Supplementary Fig. 6 and Supplementary Table 4 and 5). In DMSO-*d*₆ solution (saturated solution, ~ 20 mmol/L, 25 °C), the
36 LEDC ethylene protons give rise to a singlet at 3.63 ppm with the ethylene and carbonate carbons appearing at 62.7 and 155.2
37 ppm, respectively, which is consistent with the symmetry of the compound. In the solid state, ¹H NMR resonances appear at 3.4
38 and 2.6 ppm, which are assigned to the ethylene protons and lattice DMSO, respectively.

1 On account of its lower symmetry, the ethylene protons of LEMC appear as two triplets at 3.44 and 3.72 ppm with an
 2 OH resonance at 4.82 ppm (DMSO-*d*₆, initial concentration: 0.53 mol/L, 25 °C), with similar shifts in the solid state (Supplementary
 3 Fig. 6). The ethylene carbons and the carbonate carbon appear at 61.0, 65.8 and 156.9 ppm, respectively. However, LEMC quickly
 4 establishes an equilibrium with LEDC and EG in solution ($K_c = 0.14$), as illustrated in Fig. 4b and 4e. Adding EG or LEDC to the
 5 solutions shift the equilibria to the left, as expected. Likewise, adding EG to a pure solution of LEDC•2DMSO will generate LEMC
 6 according to the equilibrium expression (Supplementary Figure 18). These data not only establish that LEMC readily reaches
 7 equilibria in solution but also confirm the identity of LEDC through the equilibrium relationship.

8



9

10 Figure 4. Solution NMR studies on LMC, LEMC and LEDC·2DMSO. NMR spectra (500 MHz, 25 °C) of (a) LEDC·2DMSO (saturated,
 11 *ca.* 0.02 mol/L), (b) LEMC (initial concentration: 0.53 mol/L) and (c) LMC + EG (initial concentration: LMC 0.34 mol/L + EG 0.41
 12 mol/L) in DMSO-*d*₆ indicate complex equilibria. The insets in figures (b) and (c) show linear fittings used to calculate the
 13 equilibrium constants. (d-g) indicate the interconversions between these lithium organic carbonates, in reactions with alcohols
 14 and carbonate electrolytes in DMSO.

15

16 The alkyl carbonates are quite reactive towards protic solvents such as water, alcohols and the carbonate solvents EC
 17 and DMC. For example, hydrolysis of LEDC gives rise to LEMC, in both DMSO-*d*₆ solutions and the solid state (monitored by NMR
 18 and FT-IR spectroscopies, respectively. Supplementary Fig. 21-22). LEMC and LMC show much higher stability towards moisture
 19 than LEDC, but all three compounds will be hydrolyzed eventually to give corresponding alcoholic species (FTIR and simulation
 20 studies, Supplementary Fig. 23-25). In addition, the alkyl carbonates can be interconverted in DMSO solutions through the
 21 addition of complementary carbonates or alcohols. The interconversions of LMC and LEMC through the addition of EG and MeOH
 22 are illustrated in Fig. 4c and 4f with an equilibrium constant of 0.69, while the conversion of LEDC to LMC through reaction with
 23 DMC is given in Fig. 4g and NMR spectra in Supplementary Fig. 17. Dissolving LEMC and DMC together in DMSO-*d*₆ instantly
 24 results in multiple equilibria (Fig. 4 e-g) and products such as EG, LMC, LEDC and MeOH (Supplementary Fig. 20). An overview of

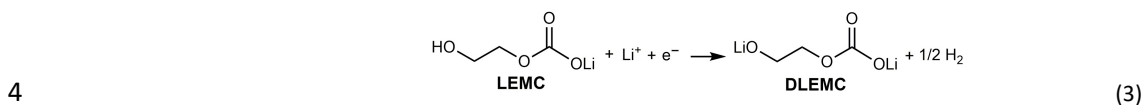
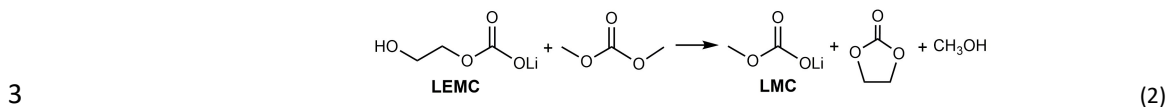
1 the interconversion chemistries that occur with LMC, LEMC and LEDC is highlighted in Fig. 4d with supporting spectra given in the
2 Supplementary Information (Supplementary Fig. 17). The interconversions *only* occur in DMSO solutions (as DMSO solvates the
3 species) and do not occur (or only occur slowly at the liquid-solid interface) when insoluble LEDC, LEMC or LMC are in contact
4 with pure EC/DMC solvents in a battery environment. Analysis of the reactions where LEDC or LEMC is suspended in DMC or
5 EC/DMC solutions (without DMSO) is presented in the supplementary information (Supplementary Fig. 26).

6
7 **Chemical compositions of SEI layers on graphite electrodes.** Because SEI layers are only 10 - 50 nm thick, isolating enough
8 material to evaluate by traditional spectroscopic methods (*e.g.* NMR) is a challenge. To overcome this problem, we fabricated
9 large and thoroughly dried electrodes containing at least 400 mg graphite (TIMREX KS44) coated on Cu current collectors (~ 200
10 cm²). The electrodes were cycled three times from 0.7 to 2.0 V vs. Li/Li⁺ to generate SEI layers. Three types of electrolytes, 1M
11 LiPF₆ in EC/DMC (v: v = 1: 1), 1M LiPF₆ in DMC and 1M LiPF₆ in EC, were used (mixing 1.52 g LiPF₆ and 13 g EC forms a liquid
12 solution at 27 °C). The electrochemical performances of the three systems are shown in Supplementary Fig. 27. When EC is
13 included in the electrolyte solutions, a plateau at ~ 0.8 V is observed in the first cycle but disappears in subsequent ones,
14 indicating the formation of SEI layers. However, when only DMC is used, no such plateau is observed. These data are consistent
15 with literature studies indicating that SEI layers are formed in the first discharge cycle and originate from EC. Previous works have
16 demonstrated continuous evolution of SEI layers during battery cycling,^{21,22} but we only focus on the initial step in SEI formation
17 here (the 0.8 V plateau in the 1st discharge process

18 The SEI films were extracted into both DMSO-*d*₆ and 0.1 M DCl in D₂O for solution NMR analysis. Representative 1D and
19 2D spectra are given in Fig. 5, Supplementary Fig. 28 and 29. Both the aqueous and DMSO extracts show significant quantities of
20 ethylene glycol bis(methyl carbonate), EGBMC, originating from catalytic reactions of EC/DMC with oxides (*e.g.* surface oxide
21 layer on Cu current collector or methoxide), which is well documented in the literature.^{38,51} The 0.1 M DCl extraction method
22 instantly hydrolyzes possible SEI candidates (*e.g.*, LEMC, LMC and LEDC) to give methanol and EG (Fig. 5b). Control experiments
23 (Supplementary Fig. 30 and 31) show that the complex equilibria and secondary chemical reactions described above are averted
24 and the observed EG: MeOH ratio provides an accurate measure of the EC-derived SEI products (*e.g.* LEMC+LEDC) : DMC-derived
25 SEI products (*e.g.* LMC) ratio present in the SEI film. The DMSO-*d*₆ extracts of SEI layers formed in 1M LiPF₆/EC/DMC electrolytes
26 contain LEMC, LEDC, EG, LMC and MeOH, as well as residual EC and DMC. NMR spectra in Fig. 5d collected on SEI layers grown in
27 the EC-only cell, where DMC, as well as DMC-related equilibria/interconversions are excluded, indicate the presence of LEMC.
28 Solid-state ¹H MAS NMR characterizations of the SEI layers coated on graphite powders, unfortunately, give very broad peaks,
29 possibly due to the presence of paramagnetic impurities in the electrodes (Supplementary Fig. 32).

30 The equilibrated DMSO-*d*₆ SEI extracts show that the primary SEI candidates (LEMC, LEDC and LMC) are indeed present,
31 but the complex equilibria and secondary reactions described above prohibit the determination of their origin (*i.e.* were they
32 present in the SEI). The hydrolyzed SEI extracts suggest that the ratio between EC-derived SEI products (*e.g.* LEMC and LEDC) and
33 DMC-derived SEI products (*e.g.* LMC) is *ca.* 5: 1 in all the repeated measurements. However, electrodes cycled in 1M LiPF₆ in pure
34 DMC result in no LMC formation and no 0.8 V SEI plateau in the first discharge cycle. These findings suggest that a significant LMC
35 component is present in SEI films but that it results from a secondary chemical reaction with LEMC or LEDC. Control experiments
36 of insoluble LEMC powders suspended in pure DMC (and EC/DMC mixture) for several weeks indicate a slow surface reaction at
37 the solid-liquid interface that transforms LEMC into LMC and EG (equation (2) and Supplementary Fig. 26). However, the

1 suspended powders are primarily LEMC after several weeks at room temperature suggesting that the particles contain a core of
2 LEMC surrounded by a thin shell of LMC. Similar chemical transformations occur with LEDC as well (Supplementary Fig. 26).



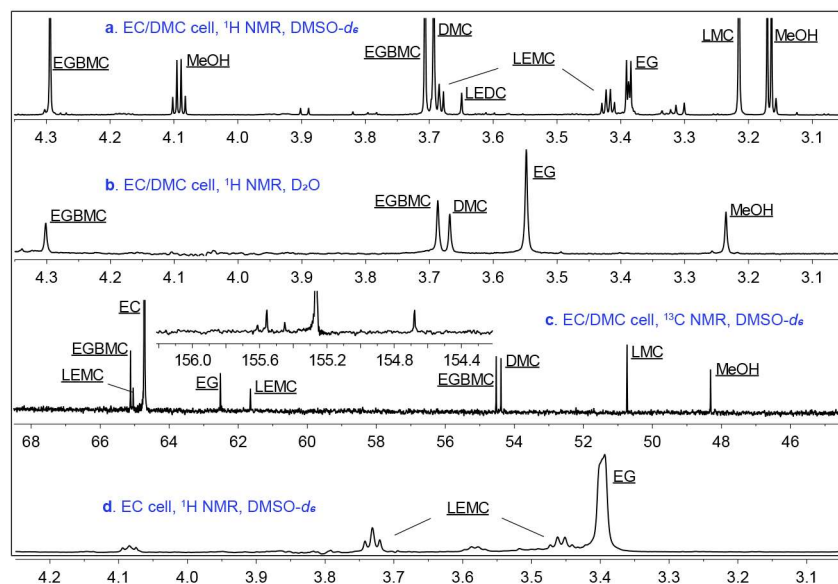
5 While we cannot unequivocally determine whether LEDC or LEMC (or both) are the initial and primary components of
6 the SEI, our hypothesis is that LEMC is the major SEI constituent and LEDC does not exist (or does not persist) in the typical LIB
7 environment. This proposal is based on the following observations: 1) A number of previous studies have linked the organic SEI
8 component to the “LEDC” standard,^{28,39,41} which was actually LEMC. 2) LEDC is highly reactive toward residual protons, which are
9 ubiquitous in all cell assemblies, from trace moisture in bulk electrolytes to surface functionalities on graphite. The presence of
10 EG (or LiEG) in the EC-only control cell (which was rigorously dried) is a direct measure of the protio impurities in battery
11 components. The protio impurities would likely convert any LEDC into LEMC. Thus, even if LEDC were formed through the single
12 electron reduction pathway (equation (1)), it is likely converted to LEMC and LMC through reactions with protons and DMC,
13 respectively, due to its inability to "survive" in the LIB environment.

14 **Formation and evolution of LEMC on graphite electrode.** While LEMC is likely a key component in the graphite SEIs, the precise
15 mechanism of its formation is still unclear. It is possible that LEDC is generated as the first step,^{10,15} but a subsequent
16 hydrolysis/protonation transforms it to LEMC, as suggested by our model chemical and computational studies (Supplementary
17 Fig. 21-22). In addition, we have discovered two alternate pathways for LEMC formation involving nucleophilic addition of OH⁻
18 (See Supplementary Fig. 33) and MeO⁻ to EC (See Supplementary Fig. 34). LiOH is a well-known component of the inorganic SEI
19 layer^{7,24} and can be converted to LEMC in a heterogeneous transformation. LiOMe is known to exist in DMC-derived SEIs^{7,24,27}
20 and its participation in electrolyte degradation through nucleophilic reactions has been thoroughly investigated.⁵¹

21 The evolution of the SEI layer with battery cycling is well known^{21,22} and reactions of LEMC are likely part of that process.
22 For example, the heterogeneous reaction of LEMC with DMC (eq. 2) forms an “LMC-capped LEMC organic layer”, which should
23 self-terminating in a dense layered structure (*i.e.* DMC cannot access the LEMC beneath the LMC surface). We believe that LEMC
24 persists in a well-functioning SEI and facilitates Li⁺ ion transfer. The well-established need for EC as the indispensable component
25 in carbonate-based electrolytes^{6,52} strongly implicates an active EC-derived compound in an effective SEI, which we attribute to
26 LEMC. The relatively high Li⁺ conductivity of LEMC likely benefits SEI function, in contrast to LMC which is a bulk insulator. The
27 alcoholic proton (R-OH) on LEMC may well be subject to electrochemical reduction, generating partially di-lithiated ethylene
28 mono-carbonate (DLEMC) and H₂ (eq. 3). Our computational studies suggest that DLEMC has equivalent or better Li⁺ ion
29 conductivity than LEMC (Supplementary Information, Section 1.7). However, we always detect a significant fraction of the
30 protonated LEMC in the electrode analyses.

31

32



1
 2 Figure 5. Solution NMR characterizations of the graphite SEI layer. Spectra (a) ^1H NMR, $\text{DMSO-}d_6$, (b) ^1H NMR, 0.1 M DCl in D_2O
 3 and (c) ^{13}C $\{^1\text{H}\}$ NMR, $\text{DMSO-}d_6$ were collected from SEIs generated in electrolyte solutions of 1M LiPF_6 in EC/DMC, while (d) shows
 4 ^1H NMR spectra in $\text{DMSO-}d_6$ of SEI layers generated in the electrolyte solution of LiPF_6/EC . NMR spectra (a)(c) and (b)(d) were
 5 collected at 25 °C with an 800 MHz and 500 MHz spectrometer, respectively.

6
 7 In conclusion, we have demonstrated, through rigorous and comprehensive characterizations including single crystal and powder
 8 XRD, FTIR, elemental analysis, solid-state and liquid 1D and 2D NMR spectroscopy, that the previously synthesized chemical
 9 standards, “LEDC”, is actually LEMC. NMR studies on the SEI layers grown on graphite electrodes in typical LIBs with 1M LiPF_6 in
 10 EC/DMC electrolyte indicate that it is highly *likely* that LEMC, instead of LEDC, prevails as the major organic component in the SEI
 11 layers. These lithium organic carbonates, including LMC, LEMC and LEDC, show complex interconversions/equilibria in DMSO
 12 solutions. In a battery environment, these compounds (*i.e.*, LEMC and LMC) appear to be formed through secondary chemical
 13 reactions and are not generated through direct electrochemical reduction. The identification of LEMC and its properties (ionic
 14 conductivity, chemical reactivity) provide insight into Li^+ ion transport across solid–electrolyte interphases and pave the way for
 15 future engineering of artificial interphases with superior properties.

16
 17

1 **Methods**

2 **General.** Details on chemical synthesis, chemical / electrochemical characterizations and SEI extractions are described in the
3 Supplementary Information.

4 **Synthesis of LMC.** All the synthetic procedures were carried out under inert atmospheres unless otherwise stated. To a Schlenk
5 flask of magnetically stirred anhydrous methanol (20 ml) at 0 °C was added 2.5 M n-BuLi/hexane (10 ml, 25 mmol) dropwise. The
6 reaction was warmed to room temperature and further stirred for 30 min. Afterwards CO₂ gas dried over a CaSO₄ column was
7 bubbled through the solution for 2 h at room temperature. The solvents were removed *in vacuo*, leaving a white powder that
8 was further rinsed with anhydrous diethyl ether. The resulting white powder was dried under vacuum for 12 h to afford LMC (1.8
9 g, 88% yield). Large needle crystals suitable for single-crystal XRD studies were obtained from a methanol/diethyl ether solvent
10 mixture.

11 **Synthesis of LEMC.** To a Schlenk flask of magnetically stirred anhydrous EG (20 ml) at 0 °C was added 1.6 M MeLi/diethyl ether
12 (25 ml, 40 mmol), or 2.5 M n-BuLi/hexane (16 ml, 40 mmol) dropwise. The reaction was warmed to room temperature and further
13 stirred for 30 min. The diethyl ether (or hexane) was removed *in vacuo*, leaving a suspension of LiEG in EG. Dry CO₂ was bubbled
14 through the suspension for 2 h under fast stirring, upon which the solid precipitates gradually dissolved and a clear but viscous
15 solution was obtained. Afterwards, anhydrous pyridine (50 ml) was added to the solution. The EG/pyridine solution was stored
16 at room temperature for 2 days under an inert atmosphere, during which time copious amounts of white powder precipitated
17 from solution. The precipitates were collected through centrifugation, rinsed with anhydrous DMF and anhydrous diethyl ether,
18 and further dried under vacuum for 12 h to afford LEMC (1.6 g, 36% yield). Large crystals suitable for single-crystal X-ray studies
19 were obtained from the solvent mixture of EG/pyridine.

20 **Synthesis of LEDC·2DMSO.** To a Schlenk flask charged with a stirred solution of LEMC (224 mg, 2 mmol) dissolved in anhydrous
21 DMSO (20 ml) was added lithium tert-butoxide (240 mg, 3.0 mmol, 1.5 equiv.) at room temperature. All powders dissolved and
22 the clear solution was stirred for 30 min. Dry CO₂ was bubbled through the stirred solution for 3 h, during which time a white
23 powder precipitated from solution. The white powder was collected through centrifugation, rinsed with anhydrous diethyl ether
24 and dried *in vacuo* for 12 h to afford white microcrystalline LEDC·2DMSO (440 mg, 68% yield).

25 **EIS measurement.** To preclude contributions from the hydroxyl protons in LEMC that may contribute to the total ionic
26 conductivities, we measured the impedance of analytically-pure LEMC pressed pellets sandwiched between two LGPS rectifiers.
27 LGPS has very high Li⁺ ionic conductivity (> 10⁻² S/cm) but does not transport protons and,^{43,44} as such, all measured transport is
28 due to Li⁺-ion conduction. A proton-blocking cell stainless steel/LGPS/LEMC/LGPS/stainless steel was assembled to measure the
29 Li ion conductivity of LEMC. The cell was prepared by cold-pressing 20 mg LGPS, 140 mg LEMC, and 20 mg LGPS powders together
30 under 360 MPa for 3 minutes. The electrochemical impedance spectrum of the cell was measured from 1MHz to 0.1Hz using an
31 electrochemical workstation (Solartron 1287/1260). The intercept with Z' axis is attributed to the resistance (R) from the bulk
32 electrolyte and grain boundaries. The ionic conductivity (σ) is determined by L/RS , where L and S are the thickness and area of
33 the electrolyte, respectively. The ionic conductivity of LMC and LEDC was also measured with the same method but without LGPS
34 as proton-blocking media.

35

1 **Data availability.** Crystallographic data for the structures reported in this work have been deposited at the Cambridge
2 Crystallographic Data Centre (CCDC) under deposition nos. CCDC 1847784 (LEMC) and CCDC 1847785 (LMC). Copies of these data
3 can be obtained free of charge via www.ccdc.cam.ac.uk/structures. Data supporting the findings of this study are available within
4 this paper and its Supplementary Information, and are available from the corresponding author upon reasonable request. The
5 MAS NMR experimental and GIPAW calculated data for this study are provided as a supporting dataset from WRAP, the Warwick
6 Research Archive Portal at http://wrap.warwick.ac.uk/**.

7

8 References

- 9 1 Winter, M., Barnett, B. & Xu, K. Before Li ion batteries. *Chem. Rev.* **118**, 11433-11456 (2018).
10 2 Yazami, R. & Touzain, P. A reversible graphite-lithium negative electrode for electrochemical
11 generators. *J. Power Sources* **9**, 365-371 (1983).
12 3 Persson, K. *et al.* Lithium diffusion in graphitic carbon. *J. Phys. Chem. Lett.* **1**, 1176-1180 (2010).
13 4 Persson, K., Hinuma, Y., Meng, Y. S., Van der Ven, A. & Ceder, G. Thermodynamic and kinetic
14 properties of the Li-graphite system from first-principles calculations. *Phys. Rev. B* **82**, 125416
15 (2010).
16 5 Goodenough, J. B. & Kim, Y. Challenges for Rechargeable Li Batteries. *Chem. Mater.* **22**, 587-603
17 (2010).
18 6 Xu, K. Electrolytes and interphases in Li-ion batteries and beyond. *Chem. Rev.* **114**, 11503-11618
19 (2014).
20 7 Verma, P., Maire, P. & Novák, P. A review of the features and analyses of the solid electrolyte
21 interphase in Li-ion batteries. *Electrochim. Acta* **55**, 6332-6341 (2010).
22 8 Dahn, J. R., Zheng, T., Liu, Y. & Xue, J. Mechanisms for lithium insertion in carbonaceous materials.
23 *Science* **270**, 590 (1995).
24 9 Levi, M. D. & Aurbach, D. The mechanism of lithium intercalation in graphite film electrodes in
25 aprotic media. Part 1. High resolution slow scan rate cyclic voltammetric studies and modeling. *J.*
26 *Electroanal. Chem.* **421**, 79-88 (1997).
27 10 Aurbach, D., Markovsky, B., Shechter, A., Ein-Eli, Y. & Cohen, H. A comparative study of synthetic
28 graphite and Li electrodes in electrolyte solutions based on ethylene carbonate - dimethyl
29 carbonate mixtures. *J. Electrochem. Soc.* **143**, 3809-3820 (1996).
30 11 Zhang, X., Kostecky, R., Richardson, T. J., Pugh, J. K. & Ross, P. N. Electrochemical and infrared
31 studies of the reduction of organic carbonates. *J. Electrochem. Soc.* **148**, A1341-A1345 (2001).
32 12 Peled, E. The electrochemical behavior of alkali and alkaline earth metals in nonaqueous battery
33 systems—the solid electrolyte interphase model. *J. Electrochem. Soc.* **126**, 2047-2051 (1979).
34 13 Fong, R., Von Sacken, U. & Dahn, J. R. Studies of lithium intercalation into carbons using
35 nonaqueous electrochemical cells. *J. Electrochem. Soc.* **137**, 2009-2013 (1990).
36 14 Nie, M. *et al.* Lithium ion battery graphite solid electrolyte interphase revealed by microscopy and
37 spectroscopy. *J. Phys. Chem. C* **117**, 1257-1267 (2013).
38 15 Aurbach, D. *et al.* The Study of Electrolyte Solutions Based on Ethylene and Diethyl Carbonates for
39 Rechargeable Li Batteries II. Graphite Electrodes. *J. Electrochem. Soc.* **142**, 2882-2890 (1995).
40 16 Winter, M., Novák, P. & Monnier, A. Graphites for lithium-ion cells: the correlation of the first-
41 cycle charge loss with the brunauer-emmett-teller surface area. *J. Electrochem. Soc.* **145**, 428-
42 436 (1998).

1 17 Winter, M. The solid electrolyte interphase—the most important and the least understood solid
2 electrolyte in rechargeable Li batteries. *Z. Phys. Chem.* **223**, 1395-1406 (2009).

3 18 Edström, K., Herstedt, M. & Abraham, D. P. A new look at the solid electrolyte interphase on
4 graphite anodes in Li-ion batteries. *J. Power Sources* **153**, 380-384 (2006).

5 19 Yoshida, T. *et al.* Degradation mechanism and life prediction of lithium-ion batteries. *J.*
6 *Electrochem. Soc.* **153**, A576-A582 (2006).

7 20 Malmgren, S. *et al.* Comparing anode and cathode electrode/electrolyte interface composition
8 and morphology using soft and hard X-ray photoelectron spectroscopy. *Electrochim. Acta* **97**, 23-
9 32 (2013).

10 21 Lu, P., Li, C., Schneider, E. W. & Harris, S. J. Chemistry, impedance, and morphology evolution in
11 solid electrolyte interphase films during formation in lithium ion batteries. *J. Phys. Chem. C* **118**,
12 896-903 (2014).

13 22 Zhuo, Z. *et al.* Breathing and oscillating growth of solid-electrolyte-interphase upon
14 electrochemical cycling. *Chem. Commun.* **54**, 814-817 (2018).

15 23 Shi, S. *et al.* Direct calculation of Li-ion transport in the solid electrolyte interphase. *J. Am. Chem.*
16 *Soc.* **134**, 15476-15487 (2012).

17 24 Zhuang, G. V. & Ross, P. N. Analysis of the chemical composition of the passive film on Li-Ion
18 battery anodes using attenuated total reflection infrared spectroscopy. *Electrochem. Solid-State*
19 *Lett.* **6**, A136-A139 (2003).

20 25 Meyer, B. M., Leifer, N., Sakamoto, S., Greenbaum, S. G. & Grey, C. P. High field multinuclear NMR
21 investigation of the SEI layer in lithium rechargeable batteries. *Electrochem. Solid-State Lett.* **8**,
22 A145-A148 (2005).

23 26 Aurbach, D. & Gofer, Y. The behavior of lithium electrodes in mixtures of alkyl carbonates and
24 ethers. *J. Electrochem. Soc.* **138**, 3529-3536 (1991).

25 27 Augustsson, A. *et al.* Solid electrolyte interphase on graphite Li-ion battery anodes studied by soft
26 X-ray spectroscopy. *Phys. Chem. Chem. Phys.* **6**, 4185-4189 (2004).

27 28 Zhuang, G. V., Xu, K., Yang, H., Jow, T. R. & Ross, P. N. Lithium ethylene dicarbonate identified as
28 the primary product of chemical and electrochemical reduction of EC in 1.2 M LiPF₆/EC: EMC
29 electrolyte. *J. Phys. Chem. B* **109**, 17567-17573 (2005).

30 29 Zhuang, G. V., Yang, H., Blizanac, B. & Ross, P. N. A study of electrochemical reduction of ethylene
31 and propylene carbonate electrolytes on graphite using ATR-FTIR spectroscopy. *Electrochem.*
32 *Solid-State Lett.* **8**, A441-A445 (2005).

33 30 Shkrob, I. A., Zhu, Y., Marin, T. W. & Abraham, D. Reduction of carbonate electrolytes and the
34 formation of solid-electrolyte interface (SEI) in Lithium-Ion Batteries. 2. Radiolytically induced
35 polymerization of ethylene carbonate. *J. Phys. Chem. C* **117**, 19270-19279 (2013).

36 31 Tsubouchi, S. *et al.* Spectroscopic characterization of surface films formed on edge plane graphite
37 in ethylene carbonate-based electrolytes containing film-forming additives. *J. Electrochem. Soc.*
38 **159**, A1786-A1790 (2012).

39 32 Ota, H., Sakata, Y., Wang, X., Sasahara, J. & Yasukawa, E. Characterization of lithium electrode in
40 lithium imides/ethylene carbonate and cyclic ether electrolytes II. Surface chemistry. *J.*
41 *Electrochem. Soc.* **151**, A437-A446 (2004).

42 33 Kang, S.-H., Abraham, D., Xiao, A. & Lucht, B. Investigating the solid electrolyte interphase using
43 binder-free graphite electrodes. *J. Power Sources* **175**, 526-532 (2008).

44 34 Liu, P. & Wu, H. Construction and destruction of passivating layer on Li_xC₆ in organic electrolytes:
45 an impedance study. *J. Power Sources* **56**, 81-85 (1995).

46 35 Xu, K. & von Wald Cresce, A. Li⁺-solvation/desolvation dictates interphasial processes on graphitic
47 anode in Li ion cells. *J. Mater. Res.* **27**, 2327-2341 (2012).

- 1 36 von Wald Cresce, A., Borodin, O. & Xu, K. Correlating Li⁺ solvation sheath structure with
2 interphasial chemistry on graphite. *J. Phys. Chem. C* **116**, 26111-26117 (2012).
- 3 37 Aurbach, D., Daroux, M., Faguy, P. & Yeager, E. Identification of surface films formed on lithium
4 in propylene carbonate solutions. *J. Electrochem. Soc.* **134**, 1611-1620 (1987).
- 5 38 Shi, F. *et al.* A Catalytic Path for Electrolyte Reduction in Lithium-Ion Cells Revealed by in Situ
6 Attenuated Total Reflection-Fourier Transform Infrared Spectroscopy. *J. Am. Chem. Soc.* **137**,
7 3181-3184 (2015).
- 8 39 Gireaud, L., Grugeon, S., Laruelle, S., Pilard, S. & Tarascon, J.-M. Identification of Li battery
9 electrolyte degradation products through direct synthesis and characterization of alkyl carbonate
10 salts. *J. Electrochem. Soc.* **152**, A850-A857 (2005).
- 11 40 Michan, A. L., Leskes, M. & Grey, C. P. Voltage dependent solid electrolyte interphase formation
12 in silicon electrodes: Monitoring the formation of organic decomposition products. *Chem. Mater.*
13 **28**, 385-398 (2015).
- 14 41 Xu, K. *et al.* Syntheses and characterization of lithium alkyl mono- and dicarbonates as components
15 of surface films in Li-ion batteries. *J. Phys. Chem. B* **110**, 7708-7719 (2006).
- 16 42 Seo, D. M. *et al.* Reduction reactions of carbonate solvents for lithium ion batteries. *ECS*
17 *Electrochem. Lett.* **3**, A91-A93 (2014).
- 18 43 Kamaya, N. *et al.* A lithium superionic conductor. *Nat. Mater.* **10**, 682 (2011).
- 19 44 Han, F., Gao, T., Zhu, Y., Gaskell, K. J. & Wang, C. A battery made from a single material. *Adv.*
20 *Mater.* **27**, 3473-3483 (2015).
- 21 45 Knauth, P. Inorganic solid Li ion conductors: An overview. *Solid State Ion.* **180**, 911-916 (2009).
- 22 46 Gurusiddappa, J., Madhuri, W., Suvarna, R. P. & Dasan, K. P. Studies on the morphology and
23 conductivity of PEO/LiClO₄. *Materials Today: Proceedings* **3**, 1451-1459 (2016).
- 24 47 Schafzahl, L. *et al.* Long-Chain Li and Na Alkyl Carbonates as Solid Electrolyte Interphase
25 Components: Structure, Ion Transport, and Mechanical Properties. *Chem. Mater.* **30**, 3338-3345
26 (2018).
- 27 48 Zhuang, G. V., Yang, H., Ross, P. N., Xu, K. & Jow, T. R. Lithium methyl carbonate as a reaction
28 product of metallic lithium and dimethyl carbonate. *Electrochem. Solid-State Lett.* **9**, A64-A68
29 (2006).
- 30 49 Pickard, C. J. & Mauri, F. All-electron magnetic response with pseudopotentials: NMR chemical
31 shifts. *Phys. Rev. B* **63**, 245101 (2001).
- 32 50 Yates, J. R., Pickard, C. J. & Mauri, F. Calculation of NMR chemical shifts for extended systems
33 using ultrasoft pseudopotentials. *Phys. Rev. B* **76**, 024401 (2007).
- 34 51 Gachot, G. *et al.* Deciphering the multi-step degradation mechanisms of carbonate-based
35 electrolyte in Li batteries. *J. Power Sources* **178**, 409-421 (2008).
- 36 52 Xu, K. Whether EC and PC differ in interphasial chemistry on graphitic anode and how. *J.*
37 *Electrochem. Soc.* **156**, A751-A755 (2009).

38

39

40 Acknowledgements

41 We thank the DOE for funding this research through the EFRC (NEES-II). B.W.E. thanks Prof. Jeffery Davis for many helpful
42 discussions. A. M. thanks the University of Warwick for a Chancellor's International Scholarship. The UK 850 MHz solid-state NMR
43 Facility used in this research was funded by EPSRC and BBSRC, as well as the University of Warwick including via part funding

1 through Birmingham Science City Advanced Materials Projects 1 and 2 supported by Advantage West Midlands (AWM) and the
2 European Regional Development Fund (ERDF). OB thanks NASA agreement NND16AA29I.

3 **Additional information**

4 Supplementary information is available in the online version of the paper. Reprints and permissions information is available online
5 at www.nature.com/reprints. Publisher's note: Springer Nature remains neutral with regard to jurisdictional claims in published
6 maps and institutional affiliations. Correspondence and requests for materials should be addressed to B.W.E.

7

8 **Author contributions**

9 B.W.E., K.X. and C.W. designed and conceived the study. L.W. directed the project and contributed chemical synthesis,
10 battery/electrode tests, FTIR and solution NMR studies. F.H. and C.W. performed ionic conductivity experiments and analysis.
11 A.M., S.P.B. and D.I. contributed solid-state NMR measurements and analysis. P.Y.Z. and Y.W. contributed single crystal growth
12 and crystallographic studies. K.G. performed XPS experiments and analysis. O.B. conducted quantum chemistry calculations.
13 B.W.E. supervised the project. All authors contributed to discussions and preparation of the manuscript.

14

15 **Competing financial interests**

16 The authors declare no competing financial interests.

17